Journal of Medicinal Chemistry

pubs.acs.org/jmc

Article

Profound Changes in Functional Structure and Dynamics of Serum Albumin in Children with Nephrotic Syndrome: An Exploratory Research Study

Haleh H. Haeri,[‖] Jana Eisermann,[‖] Heike Schimm, Anja Büscher, Peter Hoyer,* and Dariush Hinderberger*

Cite This: *J. Med. Chem.* 2023, 66, 12115−12129

Read Online

ACCESS | Metrics & More | Article Recommendations | Supporting Information

ABSTRACT: Patients with nephrotic syndrome (NS) suffer from urinary loss of albumin. As a cause, previous studies focused on the glomerular filter rather than analyzing the molecular properties of albumin itself. Later one was initiated by clinical observations indicating unexplained molecular alterations of human serum albumin (HSA) in an NS pediatric patient. Therefore, we examined serum from eight pediatric patients with steroid-sensitive and -resistant NS and compared it with serum from healthy subjects as well as commercial HSA. We used dynamic and electrophoretic light scattering to characterize the protein size and effective surface charge and electron paramagnetic resonance spectroscopy to measure the local environment and binding dynamics of up to seven fatty acids associated with HSA. Our findings suggest that pronounced differences in binding behavior and surface charge of HSA could enhance their filtration through the GBM, leading to direct toxicity of HSA to podocytes.

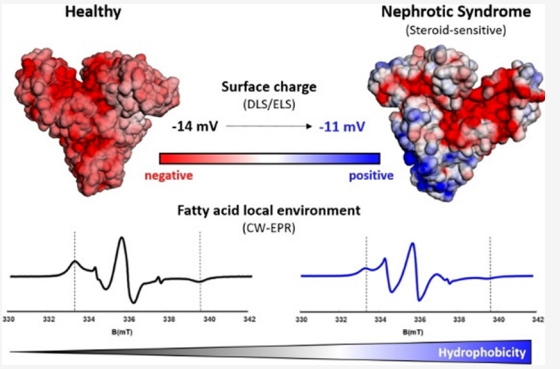

INTRODUCTION

Chronic kidney diseases (CKD) affect more than 10% of the world's population. Most of them originate from deficits in the elaborated kidney filtration barrier, the glomerulus. In the healthy state, it allows the passage of large amounts of fluid while almost completely restricting the passage of large macromolecules such as albumin.[1] The filter barrier of the glomerulus consists of three parts: the fenestrated endothelium with negatively charged glycocalyx, a negatively charged basement membrane (GBM), and podocytes, which are specialized pericyte-like cells connected via an interdigitating network of slit diaphragms.[2] Decades of research on the glomerular filtration barrier highlight the importance of all of these three layers, but the exact molecular mechanism by which macromolecules are sieved is still debated. However, one undoubtable aspect is the combined size- and charge-selective filtration of negatively charged plasma proteins.[1,3−5]

The clinical syndrome known as nephrotic syndrome (NS) shows specific features of heavy proteinuria due to an increased permeability of serum protein through the glomerulus filtration barrier (see Figure 1). The most prominent symptom, hypoalbuminemia, is frequently accompanied by dyslipidemia and edema. Renal function may be reduced, and in some cases, an immunological disorder is an underlying condition.[6−11]

Childhood-onset NS is 15 times more common than adult-onset NS and its specific origin is etiologically different. The most common causes in children (roughly 90%) are two glomerular diseases: minimal-change NS (MCNS) and focal segmental glomerulosclerosis (FSGS). Membranous nephropathy as the third distinct type is rare in children. The remaining 10% suffer from secondary NS, related to infections, systematic and immunological diseases, malignancy, and other glomerular diseases.[12] Histologically, a common feature of MCNS and FSGS is the effacement of foot processes of the podocytes detectable by electron microscopy (EM). Therefore, the culprit of the disease and the proteinuria are currently interpreted to be mediated by diseased podocytes.[13]

The common therapy for minimal-change NS relies on the use of glucocorticosteroids (like prednisone) as medication. More than 95% of the patients positively respond to it.[14] The patients with a steroid-sensitive NS (SSNS) have a benign prognosis with good long-term preservation of kidney function. Histologically, the EM shows normalization of the podocyte pathology.

A resistance to glucocorticosteroids, called steroid-resistant NS (SRNS), is defined by patients not responding after 4

Received: April 14, 2023
Published: August 30, 2023

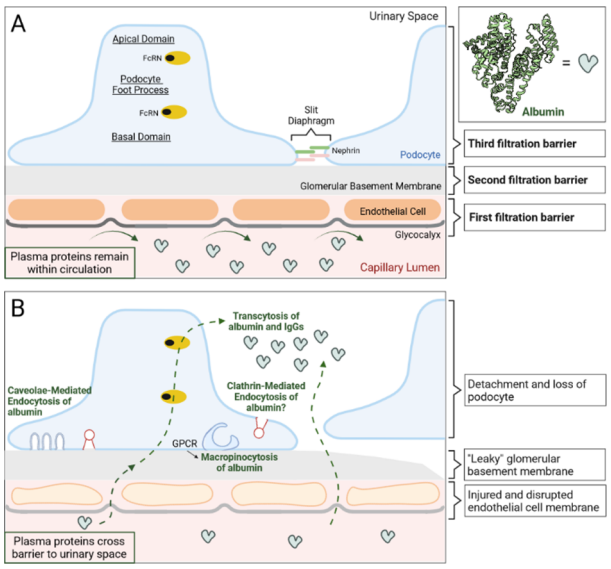

Figure 1. Schematic representation of the intact glomerular filtration barrier under the presence of proteinuria. (A) Normal components of the intact glomerular filtration barrier: capillary endothelial cells, glomerular basement membrane, and glomerular epithelial cells (podocytes) The space between foot processes are called slit diaphragm, and the podocyte foot processes are connected by nephrin molecules (red) which are essential to stabilize the podocyte cell filtration barrier. (B) Schematic representation of the proteinuria (with serum albumin)[9] from loss of the normal glomerular filtration barrier and albumin uptake mechanism by podocytes. Adapted from Refs.[10,11]

weeks of a standard course of prednisone or prednisolone and is mainly associated with FSGS. These patients have a high risk of developing chronic kidney disease.[12] FSGS may be caused by mutations of genes inducing structural and functional damage of podocytes, or secondary immune-mediated effects, which can respond to some selected immunosuppressive drugs.

An unexpected clinical finding prompted us to investigate the physicochemical structure of serum albumin in a patient with nephrotic syndrome. The index patient developed a nephrotic syndrome at the age of 1 year and 4 months. He initially received the standard therapy with prednisone but was steroid-resistant. A renal biopsy revealed a minimal change disease. Genetic testing revealed no gene mutations that have been described as causing genetic FSGS. Because of the clinical severity of the disease, he underwent a 14 month therapeutic trial with cyclosporine A (CsA), 9 plasma exchanges (PE), and most recently 3 doses of rituximab, which did not improve the clinical picture. Because of life-threatening volume overload and anasarca, his kidneys were removed sequentially at 4 years and 2 months and 4 years and 4 months, respectively. Histology revealed FSGS. The patient was placed on peritoneal dialysis. At the age of 5 years, he received a kidney transplant from a deceased donor. Initial nonfunction required 2 weeks of hemodialysis. A renal biopsy showed minimal lesions that were interpreted as early FSGS recurrence. He developed a full-blown nephrotic syndrome. High-dose CsA and intensive plasma exchanges for 4 months had no effect on his high proteinuria and critical volume overload. Therefore, PE therapy was stopped, and to normalize his serum albumin concentration (>4 g/dL) and colloid osmotic pressure, we

Scheme 1. Schematic Representation of Applied Techniques To Study Molecular Properties of Albumin[a]

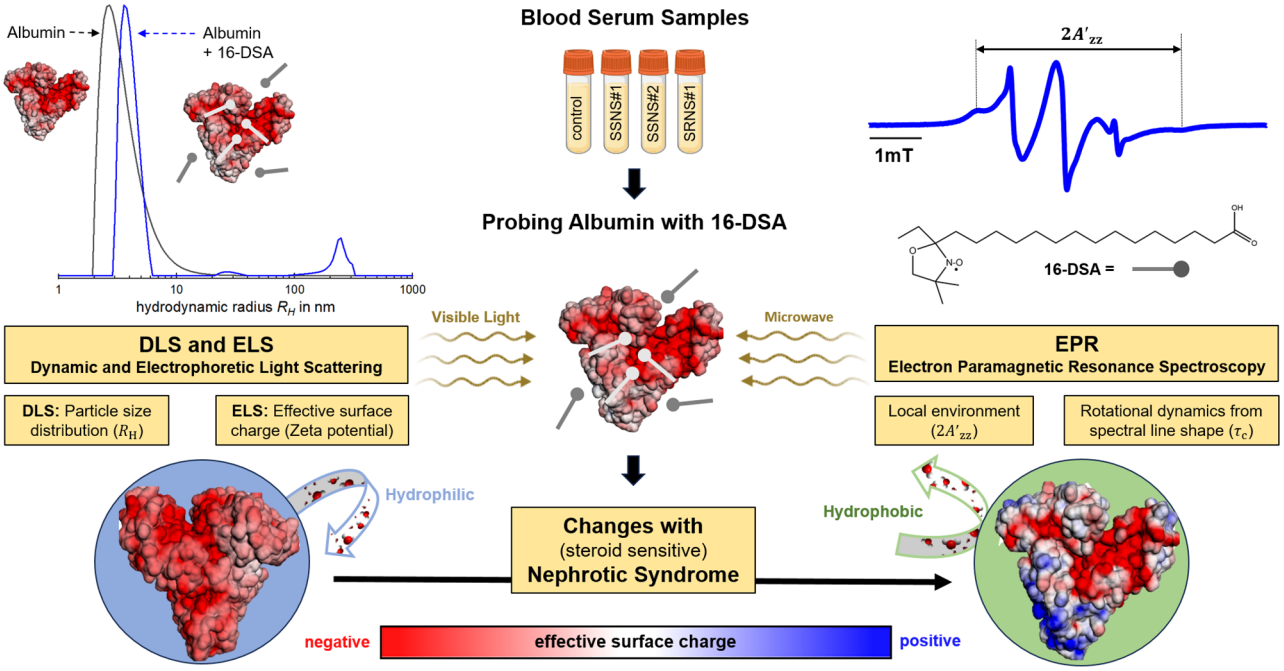

[a]Left side: Particle size distributions reflected in hydrophobic radius (R_H, pictured as a circle) for commercial HSA (~3.5 nm) is obtained by the dynamic light scattering (DLS) technique. Corresponding surface charges of HSA are provided by the ELS method and indicated in red and blue color (negatively or positively charged protein areas). Right side: A typical CW EPR spectrum of measured samples, through spin probing (16-DSA). The distance between the outermost lines of the spectrum is indicated by $2A'_{zz}$ (called apparent hyperfine coupling) which could be used as a scale of the polarity of the local environment. Spectral analysis (peak intensities and broadening) gives information about rotational dynamics (τ_c). Being more hydrophobic on the surface, water is repelled by HSA (green, apolar hydration), while in a hydrophilic case, we see the accumulation of water around protein (blue).

https://doi.org/10.1021/acs.jmedchem.3c00680
J. Med. Chem. 2023, 66, 12115−12129

Table 1. Summary of the Clinical Data for all the Tested Children Serum Samples[a]

study ID	age yr|mo	gender	weight kg	clin. diagnosis	age at onset yr|mo	PU g/g creatine	albumin g/dL	relapses	current therapy	histology
control	6|0	m		UT dilation	N/A	N/A	4.1	N/A	none	N/A
SSNS#1	1|1	m	11.0	SSNS	1|1	32.0	2.4	0	pred. altern. day	N/A
SSNS#2	13|3	m	75.0	SSNS	10|0	8.6	2.5	2	pred. full dose	N/A
SSNS#3	1|1	m	10.0	SSNS	1|1	6.6	2.3	0	pred. full dose	MCD
SSNS#4	3|5	m	13.0	SSNS[a,b]	3|5	>2.0	2.2	0	before pred. start	N/A
SSNS#5	13|11	m	84.0	SSNS	13|11	8.8	2.2	0	before pred. start	MCD
SRNS#1(mut+)	0|11	m	8.0	CNS[a,c]	0|1	2.2	3.1	0	ramipril 2.5 mg/day	FSGS
SRNS#2(mut−)	14|4	f	50	SRNS	3|0	1.1	3.9	1	pred. CsA, ramipril	MCD
SRNS#3.1(a+)	6|11	m	22.0	relapse	1|4	13.8	2.7	N/A	IS + i.v. albumin[a,d]	FSGS
SRNS#3.2(a−)	7|9		22.6	remission		N/A	4.3	N/A	IS + 4 w post i.v. alb.	
SRNS#3.3(a−)	7|11		23.0	remission		N/A	4.3	N/A	IS + 4 w post i.v. alb.	
SRNS#3.4(a+)	8|10		27.3	relapse		30.8	4.0	N/A	IS + i.v. albumin[d]	
SRNS#3.5(a+)	8|10		27.3	relapse		30.3	4.1	N/A	IS + i.v. albumin[d]	

[a]yr|mo = age in years and months, SSNS = steroid-sensitive nephrotic syndrome, SRNS = steroid-resistant nephrotic syndrome, CNS = congenital nephrotic syndrome, pred. Full dose = prednisone 60 mg/m^2 (according to ISKDC), pred. Altern. day = prednisone 40 mg/m^2 every other day (according to ISKDC), SRNS#3 represents samples from a patient with SRNS and an immediate relapse after kidney transplantation, IS = immunosuppression after kidney transplantation with prednisone and CsA, MCD = minimal chance disease, FSGS = focal segmental glomerulosclerosis. [b]This patient was diagnosed having SSNS because of his sibling having SSNS. [c]CNS with confirmed nephrin gene mutation. [d]Almost daily or every other day i.v. albumin 20% 1 g/kg body weight, 4 w post i.v. alb. = 4 weeks after the last i.v. albumin after achieving remission under i.v. albumin.

administered i.v. 20% human albumin 1 g/kg/day daily. The volume overload improved and, surprisingly, his proteinuria decreased to a normal level after 6 weeks. After discontinuation of i.v. albumin, he remained in remission for about 4 weeks but then relapsed again. After resumption of albumin infusion, he again went into remission but relapsed 4 to 5 weeks after discontinuation. This occurred about three times, so continuous therapy was initiated, with an attempt to reduce the albumin dose to 2 infusions per week. The fact that the patient's albumin was replaced by high doses of exogenous albumin led us to wonder what might be "wrong" with his albumin. A mutation in the albumin coding gene could be excluded. Therefore, investigations to characterize the physicochemical properties of albumin in patients with nephrotic syndromes were obvious.

Human serum albumin (HSA) is the most abundant and one of the most studied serum proteins[15,16] and serves a multitude of different purposes in the body. A prominent one is the transport of various compounds (e.g., fatty acids (FAs), metal ions, or antibiotic, diuretic, and chemotherapeutic as well as antidepressant drugs). Binding toxic compounds belongs to its foremost properties.[17−19] Recently, several attempts have been undertaken to monitor diseased HSA properties to understand modifications of protein function and the underlying mechanism, e.g., by disease-related posttranslational modification or by uptake of relevant biomarkers. We have developed the use of FA binding to HSA and studied its subtleties using electron paramagnetic resonance (EPR) spectroscopy, to, e.g., detect posttranslational modifications or pH-based changes in secondary and tertiary structures.[20,21] EPR is a magnetic resonance method like nuclear magnetic resonance (NMR) that detects unpaired electron spins. It has become a powerful tool not only in modern materials science and structural biology but also in biomedical applications.[22−24] Over the last years, our EPR-based studies showcase an extensive research platform focusing on HSA binding of FAs, metal cations, and pharmaceutical compounds. This platform includes the successful application of EPR to elucidate the FA binding behavior to HSA in the native serum environment and its potential use as a biological marker of, e.g., pancreatic cancer.[25,26]

For this study, we use spin-labeled FAs like 16-Doxyl Stearic Acid (16-DSA, >95%, Sigma-Aldrich, see Scheme S1) and analyze their binding behavior to HSA in human serum. This strategy enables us to obtain information on the local dynamics and conformational flexibility of the protein via the rotational correlation time (τ_c, in the picosecond to nanosecond (ps−ns) range[27]), a measure of the rotational mobility of the FAs. These data are reflected in spectral line shape, as, for example, sharp and narrow lines show free and fast rotation of spin probe (here FA), while broad lines are typically indicative of slower dynamics, due to sterical restrictions or possible binding to protein. We can also probe the local binding environment of the spin-labeled FA through the apparent hyperfine coupling (HFC, $2A'_{zz}$), which is also sensitive to rotational mobility, but also to the polarity of the local environment. $2A'_{zz}$ is defined as the separation of the two outermost features of the recorded EPR spectrum (see Scheme 1). A graphical summary of how to process an EPR spectrum is shown in Figure S2.

From a medical viewpoint, monitoring the binding behavior of FAs to albumin is also important since FAs bound to albumin increase the rate of macropinocytosis (uptake of albumin by podocytes). Moreover, FAs transported by albumin are suggested to play a leading role in tubulointerstitial injury as well as podocytes injury.[11,28−30]

The albumin surface charge affects its filtration through the anionic GBM. For example, it is reported that less negatively charged "cationic albumin" is presented in the urine of patients with NS[31] or in the case of children with membranous nephropathy. They showed high levels of circulating cationic anti-bovine serum albumin antibodies without an increase in circulating immune complex, which shows that less negative albumin or cationic albumin-antibody complexes are partially bound to the anionic GBM.[32]

To further characterize the size and surface charge of HSA, we used DLS and electrophoretic light scattering (ELS). These

https://doi.org/10.1021/acs.jmedchem.3c00680
J. Med. Chem. 2023, 66, 12115−12129

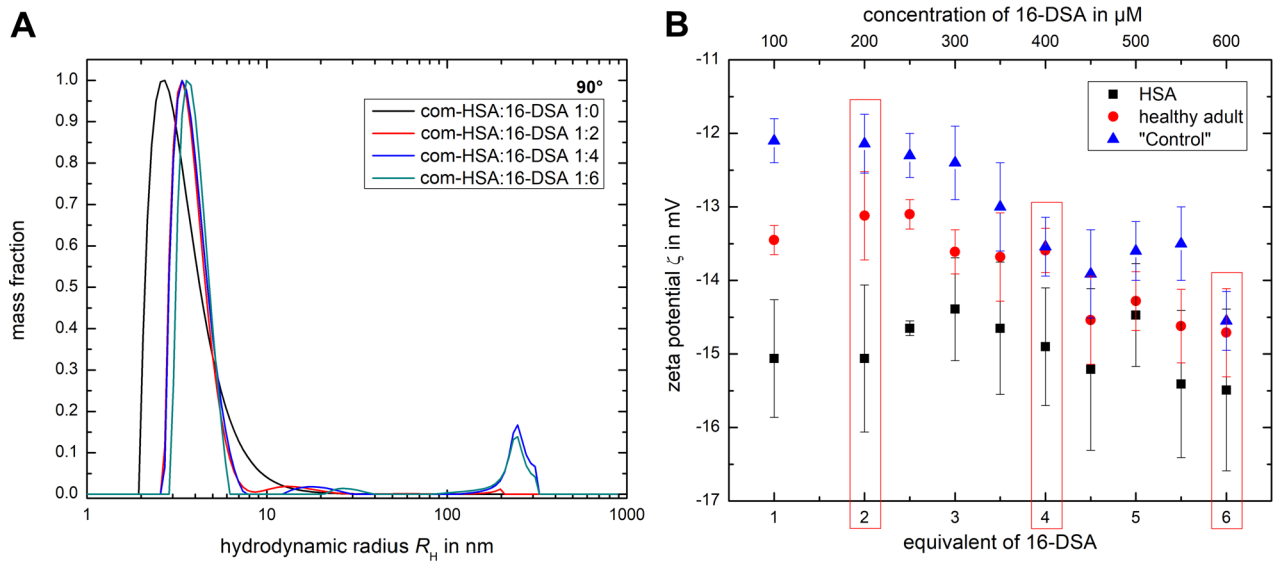

Figure 2. DLS results for com-HSA and ELS data sets for samples in the "healthy" group. (A) Particle size distribution for commercial HSA at side scattering, loaded with increasing amounts of 16-DSA. (B) Development of the zeta potential based on the added equivalents of FA for the three samples in the "healthy"-group. The three ratios 1:2, 1:4, and 1:6 are highlighted in red boxes.

methods are widely used due to their rapid and direct probing of size and surface charge of nanoparticulate matter.[33−35]

More specifically, these techniques allow for determining the hydrodynamic size and the electrokinetic potential of albumin inside the respective serum samples. The latter is a measure of the effective charge, also known as zeta potential, of HSA molecules in solution and therefore serves as a valuable parameter to unravel changes in the charge distribution of albumin for patients with NS.[36,37] Scheme 1 gives an overview of how our used characterization methods are linked together.

In the following, we will show that by combining the results from EPR spectroscopy and the applied light scattering techniques (DLS and ELS), we are able to provide insight into the dominant protein−FA interaction patterns on a nanoscopic scale. The stepwise increase in 16-DSA content (covering loading ratios of 1:1 to 1:7 for HSA:16-DSA) allows us to populate at least seven binding sites for FAs present and HSA. We can monitor to what extent local charge distribution, immediate HSA environment, and its dynamics in serum samples of children diagnosed having NS diverge from the corresponding values for the protein of healthy individuals. Finally, we attempt to understand and characterize the molecular origins of these differences and discuss the implications for the pathophysiology of different forms of NS and effects like toxicity for podocyte functions.[11]

RESULTS AND DISCUSSION

We first present the results obtained from DLS, ELS, and EPR for all examined samples at different loading ratios. We display the results according to the clinical status of the respective patients: group 1: "*healthy*", i.e., no kidney disease/no elevated urinary protein/creatinine ratio, group 2: SSNS, group 3: SRNS. We then discuss all experimental data together and draw conclusions on their interpretation considering, as far as it is possible with our in vitro methods, the medical aspects. An overview of the clinical data related to the tested serum samples is given in Table 1.

Light Scattering Measurements. *Group 1—No Proteinuria.* Before performing experiments on serum samples, we tested our approach on commercial HSA (lyophilized powder, purified to 99%, FA-free, Sigma-Aldrich). Initially, we aimed at understanding if dilution had any effects on particle size distributions in DLS measurements. Hence, we compared DLS data obtained for a buffered aqueous 120 μM HSA solution, to a sample diluted to 30 μM. We did not observe significant effects on the particle size distribution by DLS. Both side- and backscattering present a monodisperse distribution with a maximum value for the hydrodynamic radius of around 3.5 nm, which fits nicely with values given in the literature and our own reported findings.[38] The calculated zeta potential of commercial HSA without FAs amounts to −10.5 mV (Figure S1 and Table S1).

The obtained DLS-based particle size distributions for the loading ratios 1:2, 1:4, and 1:6 are depicted in Figure 2A. As soon as FAs are added to the albumin solution, particle size distributions are not monodisperse anymore. The peak maximum of the size distribution shifts to slightly larger hydrodynamic radii ($R_H \approx 4$ nm), indicative of a pronounced interaction between the initial individual albumin molecules (unimers) and 16-DSA. By increasing FA concentrations (higher loading ratios), the position of the hydrodynamic maximum does not change significantly. Higher amounts of FA affect the particle populations with flat peak positions around 20 nm and above 100 nm, revealing the formation of FA micelles and potentially of aggregated commercial purified albumin species. However, these species only represent a minor component inside the tested samples, which were still dominated by albumin unimers.

Addition of FAs to the com-HSA solutions does not only increase the hydrodynamic radius for the com-HSA but also leads to modified electrokinetic (zeta) potentials in the albumin solutions. Throughout all examined loading ratios of HSA:16-DSA, the zeta potential remained (within the margins of error) at a value of −14.9 ± 0.8 mV, as shown in Figure 2B. Similar to the DLS results, there is a significant change between loaded albumin and pure albumin solution, but no changes due to the increased amount of 16-DSA. The latter is

https://doi.org/10.1021/acs.jmedchem.3c00680
J. Med. Chem. 2023, 66, 12115−12129

expected since the charge stability of the protein improves by taking up few FAs already.[39,40]

These measurements mainly serve as a reference for the diseased serum samples that contain a more complex composition, aggravating the analysis of albumin under different FA loading ratios. To unravel if differences in the zeta potential of albumin in serum are due to (a) the serum environment or (b) a modified behavior of albumin itself, measurements with serum samples from a healthy adult and healthy juvenile patient were performed, as well. Note that albumin by far is the majority component of protein in blood serum and we have established that the FA binding in serum is dominated by binding to HSA. The developments of the zeta potential for all three samples collected in the "healthy" group (without PU) are summarized in Figure 2B. By comparing the commercial HSA solution with the two patient groups (SSNS and SRNS), the three loading ratios 1:2, 1:4, and 1:6 can be seen as specific landmarks to discuss similarities as well as differences between these groups. At a 1:2 loading ratio, the juvenile control samples without PU show the most positive zeta potential, followed by the healthy adult sample. Both zeta potentials in blood serum are significantly different from commercially available HSA in solution. Increasing the loaded FAs to four, both serum samples present similar electrokinetic (zeta) potentials, which are still more positive (~1−3 mV) compared to HSA. Moving toward a 1:6 loading ratio, all three samples display similar zeta potentials, within the margins of their error. These results are consistent with the fact that HSA gains structural and charge stability by uptake of FAs.

It should be mentioned that the loading ratios only consider the 16-DSA that was purposefully added to the sample. In contrast to the commercial HSA, which does not contain other FAs capable of interacting with albumin, the serum contains other FAs or compounds that can bind to albumin (specifically or non-specifically). Therefore, the actual number of available binding sites for added FAs might be reduced due to competitive binding of naturally occurring FAs to albumin in the serum. In addition, other (smaller) serum constituents can block potential binding sites for external, added FAs. This can explain the drastic drop in the zeta potential when increasing the loading ratio from 1:6 to 1:7, as visible for, e.g., the healthy adult sample changing from −14.7 to −16.6 mV. This behavior indicates that compared to FA-free com-HSA solutions, in serum samples, albumin has a lower number of binding sites accessible to FAs. The zeta potential of albumin from the serum samples is in general less negative when compared to com-HSA, especially for low loading ratios, which could be due to forced conformational changes (or restrictions) upon FA binding for HSA in the actual serum samples. One should furthermore keep in mind that serum also contains minor nonalbumin components that may slightly change the zeta potential, and whose relative influence is larger at low loading ratios and FA concentrations. At loading ratios higher than 1:3, the trends are similar in all three serum-based samples of this group and the absolute values grow closer.

Group 2—SSNS. The zeta potential results for serum samples in the SSNS group are summarized in Figure 3. For the three highlighted loading ratios, SSNS#2, SSNS#3, and SSNS#5 samples behave similarly such that the zeta potential is (a) constant with an increasing amount of FA and (b) its value is significantly more positive compared to the "healthy group" samples. Moreover, these three samples possess matching PU values, which indicate a comparable loss of albumin.

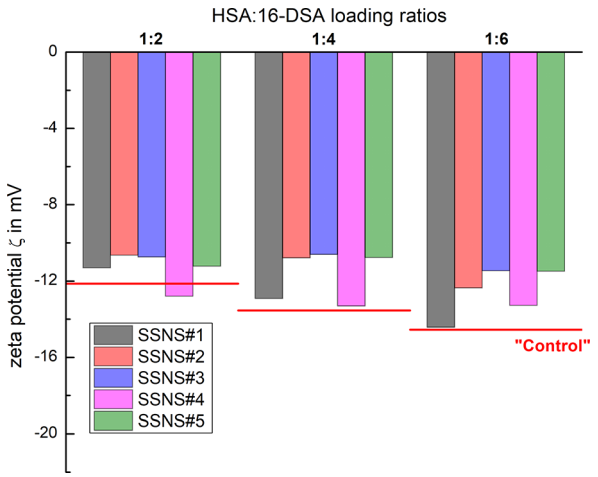

Figure 3. ELS results for samples in the SSNS group. Comparison of the zeta potential at three loading ratios for all children's serum samples diagnosed with SSNS. As a reference, the zeta potential for the "Control" sample ("healthy"-group) is shown as a red bold line.

In sample SSNS#4, albumin also shows a constant zeta potential (within the established margin of error of ±1 mV) with increasing loading ratios, which is more negative compared to the other samples in this clinical group. The PU is much lower and at the threshold defining this as nephrotic PU, indicating the beginning of the remission. A possible explanation is that similar to functional HSA of the "healthy" group, the more negative zeta potential of SSNS#4 even at low FA ratios prevents its filtration through the negatively charged GBM of the glomerular filtration barrier.

With respect to the other SSNS-group samples, the SSNS#1 sample has a different trend. Similar to the "Control", its zeta potential gradually reaches more negative values with increasing 16-DSA content. Its PU value is about 4-fold higher than for SSNS#2/#3/#5, which correlates with a more severe loss of albumin. With that, one might conclude that a high PU value is promoted by less negative, more positive electric potential values of HSA at lower FA loading ratios.

Group 3—SRNS. This group comprises three samples, measured values for the two samples SRNS#1-mut+ and SRNS#2-mut− are summarized. For the third patient/sample, SRNS#3, we obtained five different specimens taken from the patient during treatment time. Therefore, this sample, which presents a severe case of SRNS, is discussed separately. SRNS#1-mut+ is the only sample where a podocyte disease-causing mutation in the nephrin gene *nphs1* was found. Normal nephrin expression in the slit diaphragm is essential for the proper function of the renal filtration barrier. Mutations cause congenital NS of the Finnish type.[41] The measured zeta potential values (see Figure 4A) turn more negative at loading ratios 1:4 and 1:6. A possible explanation that, of course, which is highly speculative at this point, could be that given a normal distribution of HSA charges, the more negative HSA is retained and counteracts/compensates the protein loss due to the mutation. Built on this, the distribution of HSA-types in the serum of SRNS#1-mut+ might be skewed, as less negative HSA might be preferentially lost, and the retained HSA is more negative HSA with increasing 16-DSA content, whereas the absolute value is higher compared to all the previous samples of all groups.

https://doi.org/10.1021/acs.jmedchem.3c00680
J. Med. Chem. 2023, 66, 12115−12129

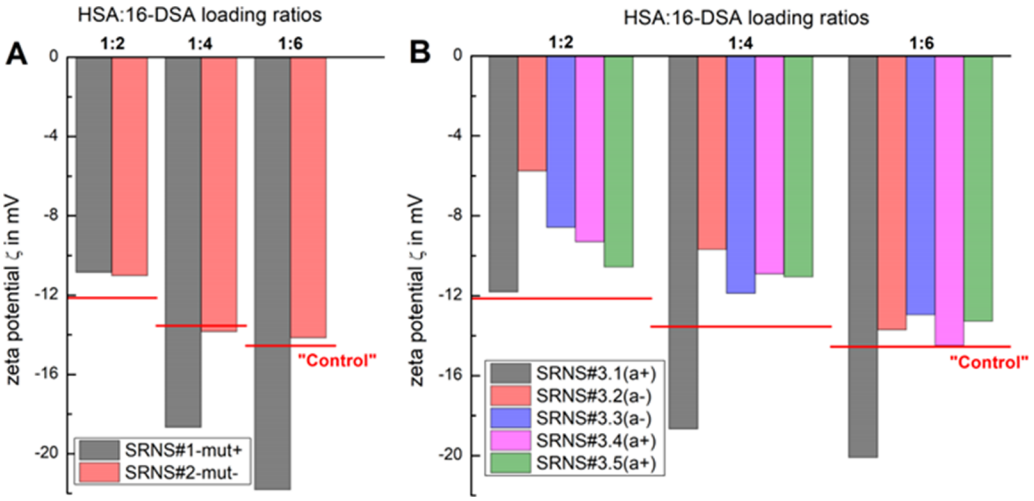

Figure 4. ELS results for samples in the SRNS group. (A) Comparison of the zeta potential at three loading ratios for all children's serum samples with SRNS. (B:) Change in zeta potential depending on the treatment state of the patient with severe SRNS (sample SRNS#3.1). As a reference, the zeta potential for the "Control" sample ("healthy" group) is shown as a red bold line.

The sample SRNS#2-mut− does not show significant differences as compared to the reference "Control" sample (see Figure 4A) and behaves similarly to the samples in the "healthy" group. It is of note that he is histologically classified as FSGS; however, clinically, his PU of 1.1 g/g creatinine is below the nephrotic range PU of >2.0 g/g creatinine, and his HSA concentration is within the normal range. Therefore, a deviation from control samples was less likely or unlikely.

All SRNS#3 patient samples are from different clinical and therapeutic conditions after a relapse of the original FSGS disease after kidney transplantation with phases of PU relapses and remissions. The first sample denoted as "SRNS#3.1(a+)" was taken when the patient was under high almost daily albumin infusion but still has a high PU and a low albumin concentration, both in the nephrotic range. In this sample, the albumin molecules exhibit a significantly more negative zeta potential, especially at loading ratios 1:4 and higher. This suggests that the fraction of HSA in the patient is dominated by the infused normal albumin and, therefore, is the main contributor to the almost normal negative zeta potential.

All the other SRNS#3 samples show a reduced (more positive) zeta potential. For the SRNS#3 series of samples, we noticed that (a) at low concentrations of 16-DSA (loading ratio 1:2), the zeta potential for SRNS#3.2(a−) and SRNS#3.3(a−) is even less negative than for the diseased serum sample of the SSNS group. Both samples are taken after albumin was administrated intravenously 4 weeks before. Moreover, by (b) increasing the concentration of 16-DSA (loading ratio 1:6) drifted the zeta potential to a negative value close to the "healthy-group "control" sample. Note that here the variance between the samples SRNS#3.2 and 3.5 is the least pronounced and in the margin of error (±1 mV) for the applied measurement setup (Figure 4B).

Figure 5 summarizes the measured median zeta potential values for the two patient groups SSNS and SRNS as a function of the FA loading ratio. Due to the variety in clinical conditions in the SRNS group, SRNS#1 and SRNS#2 are excluded for reasons explained, representing different FSGS entities, i.e., SRNS#1 having a causative nephrin mutation, and SRNS#2 presenting not in a clinical nephrotic state. We choose to take SRNS#3.2−3.5 samples into account while

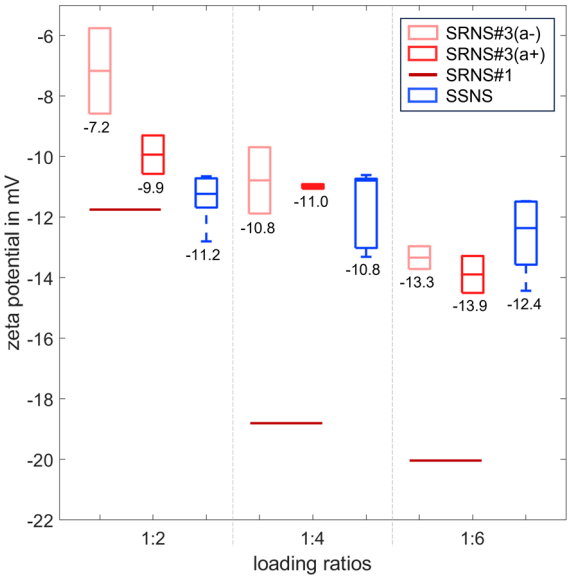

Figure 5. Boxplots of ELS results for group SSNS and severe SRNS case (SRNS#3). Light and dark red boxes show zeta potential at different loading ratios for SRNS#3 samples, separated based on the remission state (a− with 4 weeks after the last HSA substitution; a+ under HSA substitution). SRNS#3.1 is taken separately and shown as an orange line. Blue boxes present results for the SSNS group. The medians (lines in boxes) and their corresponding values are given in all plots.

showing SRNS#3.1(a+) as orange lines in Figure 5). For a loading ratio of 1:2, all groups show a more positive zeta potential for their serum (dominated by albumin) compared to samples belonging to the "healthy" group. The observed trend in the zeta potential is SRNS#3(a−) < SRNS#3(a+) < SSNS. Samples belonging to the SRNS#3(a−) group were measured 4 weeks after the last albumin infusion; with a half-life time of around 12−19 days, the majority of the exogenous albumin fraction is thus gone. The disappearance of "normal" serum albumin correlates with a shift in the zeta potential to more positive values. Under daily albumin injections ((a+) group), its charge stability improved even for a low FA content.

https://doi.org/10.1021/acs.jmedchem.3c00680
J. Med. Chem. 2023, 66, 12115−12129

Increasing the ratio to 1:6 levels out the initially visible differences between all groups.

EPR Measurements. We mainly discuss the results for the 1:4 loading ratio of HSA:16-DSA as it is the one with the most prominent changes of EPR characteristics in both, serum-based and com-HSA-based samples.[25,26] Unless significant differences are observed, the results for the two other loading ratios are given in the SI. All reported values are the median values as medians are found to be statistically robust against outliers and we can monitor the trends of modifications.[25,26] The five different SRNS#3 samples are also discussed separately to observe the characteristic EPR trends, if there are any, during the course of treatment.

Simulation of EPR spectra enables us to monitor the protein binding behavior in terms of actual FA species binding to the sites. In our analyses of serum-based FA binding to HSA,[25,26] we have established analysis of FA species that are strongly restricted in their rotational mobility (denoted "strongly bound" site "A") and an FA species that is intermediately restricted in rotational mobility ("intermediate" binding site "B"). In addition to the spectroscopic variables, population estimation of each of the two binding sites or their relative contribution to the overall spectrum could be obtained, based on their double integration value of the EPR spectrum for each of the three components.[26] This is the common variable for the quantification of spectral components. The experimental and simulated CW EPR spectra for all samples at the loading ratio of 1:4 are given in the main text (see Figure 6). As can be seen, there are distinct differences in the EPR spectra of the SSNS and SRNS groups. All other EPR spectra and their simulations (loading ratios 1:2 and 1:6) are shown in the SI (Figures S3 and S4). The corresponding numerical values obtained by simulations for the 1:4 ratio are given as an instance in Table 2. Information on two other ratios is collected in Table S2.

Group 1—No Proteinuria. Our group has conducted a detailed study of the EPR spectral patterns of the com-HSA, commercially available purified, FA-free HSA and HSA in the serum of healthy adults.[25] We could characterize the effect of serum on the binding behavior of FAs to HSA and observed that the 1:4 loading ratio could be considered the critical ratio at which EPR characteristics (like HFC and τ_c) are significantly affected.

Although the "control" sample stems from a juvenile patient with no symptoms of proteinuria, the EPR spectroscopic data reveal different behavior from the healthy adult samples regardless of the loading ratio. For example, both binding sites of the juvenile control sample are more water-exposed (higher HFC values) and have faster dynamics, compared to the healthy adult sample (see Table S2).

Group 2—SSNS. The largest differences in the SSNS group as compared to the healthy juvenile and adult groups are observed for binding sites (A). Although 16-DSA experiences rather similar environments (based on the HFC median values), one should be aware that FA binding to albumin is dynamic, and that 16-DSA bound to serum-based HSA has a ∼5 ns faster rotational dynamics compared to all reference samples, com-HSA, healthy adult, and healthy juvenile samples without PU. There are no significant changes in the properties of the (B) sites, neither in terms of their HFC nor in terms of their dynamics.

Group 3—SRNS. As mentioned above, patient SRNS#2-mut− had been diagnosed with FSGS type of NS, however, with a low PU and normal serum albumin concentration when

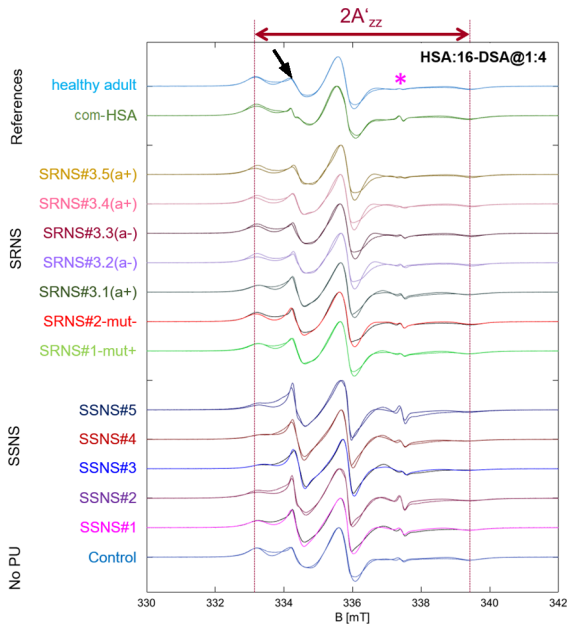

Figure 6. Experimental and simulated CW EPR spectra (colored per sample, plotted against magnetic field B in milliTesla, mT) for children's samples at a loading ratio 1:4. Two distinguishable features between SSNS and SSRS groups can be pointed out. First, there are different spectral line shapes, indicating different binding behavior of 16-DSA to HSA (arrows, asterisk, and full lines). The black arrow shows faster dynamics of a rather loosely bound FA to protein for all SSNS samples. The second feature relates to the amount of free FA (not bound, see asterisk). Spectral simulation allows the quantification of these differences. The apparent hyperfine coupling ($2A'_{zz}$) is indicated as the distance between the two outermost lines. The "healthy adult" data set represents a healthy individual adult as described in refs 25, 26.

the sample was taken. We did neither observe a significant deviation in the HFC at both binding site values nor in the charge from ELS when compared to a healthy adult, healthy juvenile, or com-HSA, as expected. However, this sample shows faster FA-dynamics in (B) sites and has a bigger hydrodynamic radius.

Since five samples were provided for patient SRNS#3, we report the median of the values, so that the SRNS#3 set of samples could be compared with two other samples in this group, as well as the individual values of SRNS#3 samples so that we can monitor the proceeding of medical treatment of the patient through the samples.

The SRNS#1-mut+ and SRNS#3 samples show some similarities; they have faster FA-dynamics at both binding sites, and both show strong deviation from normal charge state, however, in different directions. While SRNS#1-mut+ bears more negative zeta potential, SRNS#3 samples have more positive effective charges. Again, from (A) sites to (B) sites, the shift in the HFC indicates a lower polarity/hydrophilicity of the binding sites that is much more pronounced for SRNS#3 samples (decrease in $\Delta 2A'_{zz}$ ∼13 MHz vs ∼3 MHz for SRNS#1-mut+). These findings suggest that especially sites (A) of albumin, the strongly immobilized FA sites, are affected in the SRNS#3 samples.

Insight from Samples with HSA:16-DSA Loading Ratio 1:4. The differences and (when existing) similarities between the two diseased (SSNS/SRNS) groups in terms of their local surface charge (reflected in their zeta potential),

https://doi.org/10.1021/acs.jmedchem.3c00680
J. Med. Chem. 2023, 66, 12115−12129

Table 2. Summary of EPR Spectral Simulation Parameters and Light Scattering Results for HSA:16-DSA Loading Ratio 1:4. EPR Parameter Sets Are Separated Based on Binding Site and Including the Apparent Hyperfine Coupling $2A'_{zz}$, the Rotation Correlation Time τ_c, and the Contribution (Cont.) of each Component[a]

HSA:16-DSA 1:4											
	site (A)			site (B)			free FAs			charge	size
sample	$2A'_{zz}$ (MHz)	τ_c (ns)	cont. (%)	$2A'_{zz}$ (MHz)	τ_c (ns)	cont. (%)	$2A'_{zz}$ (MHz)	τ_c (ns)	cont. (%)	zeta potential (mV)	R_H (nm)
control	97.00	11.33	75.14	95.20	4.42	24.41	98.80	0.04	0.44	−13.54	3.72
SSNS#1	97.80	9.43	73.00	92.70	3.11	26.30	100.40	0.04	0.69	−12.92	6.84
SSNS#2	101.80	7.22	74.62	90.70	5.00	24.02	100.10	0.04	0.13	−10.79	7.61
SSNS#3	95.70	6.48	63.78	88.70	2.07	36.76	102.40	0.04	0.45	−10.61	8.07
SSNS#4	92.50	6.68	69.66	88.70	3.20	29.34	101.40	0.04	0.10	−13.31	7.64
SSNS#5	98.70	7.24	61.12	88.70	5.45	37.00	97.80	0.04	0.18	−10.77	8.30
SRNS#1-mut+	97.70	8.16	81.36	93.70	2.07	18.43	101.40	0.04	0.19	−18.67	3.72
SRNS#2-mut−	97.40	13.45	83.78	91.10	2.58	16.51	97.80	0.04	0.40	−13.84	6.11
SRNS#3.1(a+)	97.70	8.16	76.20	93.70	2.07	23.50	101.40	0.04	0.29	−18.67	5.79
SRNS#3.2(a−)	102.50	8.50	82.85	88.60	2.71	16.95	96.00	0.04	0.19	−9.69	6.95
SRNS#3.3(a−)	100.00	9.00	85.69	88.60	2.48	14.03	98.80	0.04	0.27	−11.88	4.49
SRNS#3.4(a+)	101.30	10.88	84.03	88.60	2.84	15.89	94.00	0.04	0.07	−10.91	4.27
SRNS#3.5(a+)	102.50	8.86	84.50	88.60	2.71	15.30	97.40	0.04	0.20	−11.06	6.94
com-HSA[b]	97.10	12.84	86.00	91.50	3.24	13.60	101.40	0.04	0.33	−14.90	3.84
healthy adult[c]	95.10	15.15	78.30	88.60	4.21	21.60	98.40	0.04	0.10	−13.59	3.28

[a]Charge/size estimations (by DLS/ELS) are given for completion. [b]Purified commercial HSA sample. [c]Sample from the healthy adult group in ref 25.

their local binding site environments, and their FA dynamics are discussed using biological aspects. The diverse samples of SRNS#3 reflect serum at different stages of disease and treatment and allow tracking of the effects on albumin during treatment time. We classified the samples in the diseased groups based on their EPR-spectroscopic characteristics in a manner similar to our established approach.[25,26]

We find that EPR and ELS results of the control group show different trends when 4 eq of FAs are added; while the zeta potential (which is a single parameter averaged over the whole ensemble of albumin molecules) becomes similar to values of com-HSA, this is not the case for the EPR-based characteristics (that give different values for different ensembles of spins) more local, nanoscopic view).

In samples of the SSNS group, there is a decrease in hyperfine coupling values from site (A) to site (B) which indicates more hydrophobic local environments. In the context of proteins and amino acids, the more positive zeta potentials (compared to the reference samples) of the samples in this group are consistent with reduced local pH values, which in turn lead to lower HFC in EPR spectra of nitroxide-labeled FAs.[42,43]

Monitoring the populations of each binding site, we found that regardless of the loading ratios, SSNS group samples have (A) sites less populated with 16-DSA than corresponding sites of the SRNS group samples. This is derived from their spectral contribution and may either indicate a tertiary structure difference, e.g., by PTMs, that shifts binding to B-sites in the SSNS group samples or competitive binding of, e.g., biomarkers at A-sites.

The corresponding plot for the 1:4 ratio is given in Figure 7 (the other two ratios are plotted in the SI as Figures S5 and S6). Clearly, the SSNS and SRNS group samples can be distinguished in this plot of spectral contributions vs rotational correlation time τ_c.

We observed an FA-dependent change in the electrokinetic potential for the samples in the SSNS group, which all were significantly more positive compared to the set of reference

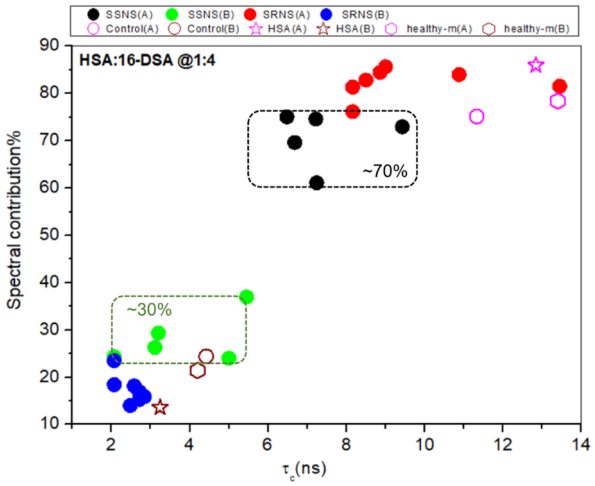

Figure 7. Different behavior of HSA's two binding sites with 16-DSA, at a loading ratio of 1:4 HSA:16-DSA. Based on the information obtained from spectral simulations, we can estimate the population (spectral contribution) of each binding site (A) and (B) (please see text), as well as dynamics (τ_c (ns)) for samples. The SRNS group contains all SRNS#3 sets of samples. "Healthy-m" denotes the median values for all healthy samples per binding site and "HSA" show the values for commercially purified HSA, according to ref 25.

samples. A more positive zeta potential for albumin, flanked by a changed binding behavior between the protein and FAs, can be the cause for its increased loss and therefore higher PU values. In the case of the SRNS group, we did not observe similar trends. However, the underlying treatment is different and SRNS#3, e.g., had been administered high doses of exogenous albumin.

From a molecular point of view, the strong affinity binding sites are reported to be located in domains 2, 4, and 5 of HSA, which have FAs bound to R (Arginine), K (Lysine), S (Serine), and Y (Tyrosine) residues through their head groups.[44,45] The apparent modification of the HSA charge

https://doi.org/10.1021/acs.jmedchem.3c00680
J. Med. Chem. 2023, 66, 12115−12129

toward a less negative zeta potential may lead to the failure by the reduced repellent electrostatic forces by the negative GBM filtration barrier. The change of the charge state could be due to alterations of the highly dynamic solution surface structure of HSA[20] and a subsequently different surface exposition and surface potential of the charged amino acids.

SRNS#1-mut+ is a mutated nephrin case, and as shown in Figure 4 and Table 2, it displays much more negative zeta potentials than the control (−18 to −20 mV). The difference in local hydrophobicities between (A) and (B) site-bound FAs is only about 3 MHz, which is significantly (three times) lower as a relative change when compared with the corresponding values in the SSNS group.

The EPR data indicate that in SRNS#1-mut+ FA binding sites, the EPR-active nitroxide moieties report less hydrophobic environments, which can be due to, e.g., higher local water exposition, higher "local" pH, and negative charges (deprotonation of carboxylic acid functionalities of the FAs). HSA is known to "pre"-bind amphiphilic substances at hydrophobic patches on its surface, which also contributes to the found (B) sites and the higher $2A'_{zz}$ value.[20] Altogether, at this point, one may speculate that local structural changes that include changes in zeta potential and dynamic FA binding might counteract the reduced functionality of the GBM in this patient. Or it is a consequence of charge selectivity in that way that preferentially less negatively charged albumin passes the GBM.

Patient SRNS#2-mut− suffers from FSGS, in which lesions affect some parts of the podocytes. Therefore, the renal system does not have its full operational functionality. At this point, we may speculate that due to this partial damage/injury to the podocytes, we may observe partially different experimental variables compared to the healthy adult or the juvenile control patient samples. Indeed, we find that bound 16-DSA dynamics and HSA particle size diverge to some extent from those of our reference group, but we did not observe significant deviations in its local environment around both binding sites.

We also monitored the behavior of nonbound or free FAs, since high amounts of nonbound 16-DSA even at low loading ratios indicate loss of binding sites and can hence be considered as a malfunction of HSA, e.g., by misfolding.[46−49] As expected, by increasing the loading ratios of FAs, both groups show an increase in the amount of free FAs. This rise, however, is roughly twice as large for the SSNS group, when compared with SRNS group samples, reaching values up to ∼2% for some SSNS samples (see Figure S7). This finding can be rationalized when considering that the prescribed steroids as potential ligands occupy HSA binding sites (Sudlow sites 1/2, see e.g., ref 9) and block several FA binding sites. This obviously is particularly true for the samples of patients that respond to treatment with steroids. It is noteworthy that the median amounts of free FAs stay below 1% for healthy samples, even at a loading ratio of 1:7.[25]

In this regard, there is also a distinct difference between the SSNS and SRNS groups. Although all SRNS samples show two times lower amounts of free FAs (at all loading ratios) compared to SSNS group samples, these amounts are still higher than those of the healthy control group. The free components per classified group are shown in Figures S8 and S9 Scatter dot plots of dynamic variation of FA bindings at different loading ratios of HSA:16-DSA are shown in Figures S11−S13.

SRNS#3 Sample Comparison at Different Loading Ratios in Course of Time (2017−2019). *HSA:16-DSA 1:2.* While the FAs in all SRNS#3 samples show faster dynamics than the juvenile control sample (for both binding sites faster by ∼2 ns), they do not show significantly different dynamics from healthy adult samples. Also, there are no significant differences between HFC of (A) binding sites compared to juvenile or healthy adult controls. However, at their (B) sites a decrease of $\delta(2A'zz)$ by 6−8 MHz as compared to all reference samples could be found (see Figures S10 and S11). Such a significant decrease in HFC indicates significantly more hydrophobic, less water-accessible states for these binding sites, as compared to normal conditions. EPR observations are well accompanied by ELS data (Figure 5) which, as explained above, are indicative of highly more positive zeta potentials for both, SRNS 3(a−) and 3(a+) (−7.2 and −9.9 mV).

Since these changes are remarkably persistent throughout time and disease/treatment status (monitored during 2 years), this could indicate that the origin of these changes is truly due to a persistent/permanent change in HSA properties in this patient. Since no mutation in the gene encoding for HSA is found, one may conclude that these changes are either induced by persistent binding of other ligands/biomarkers or posttranslational modifications that prevail in the serum of this juvenile patient.

HSA:16-DSA 1:4. Compared to the reference samples, an increase of $2A'_{zz}$ of 16-DSA bound to (A) sites of about 5−7 MHz indicates a more water/serum exposed dynamic positioning of the nitroxide at the FA ends (position 16, Scheme S1). Replacement or displacement of water as a binding site ligand to the bulk water (solvent/buffer) and vice versa could be accompanied by large energy differences which in turn can lead to major structural rearrangements.[50] This means that a supposedly permanent change of albumin binding behavior (observed at 1:2 loading ratios) may implicate further structural changes at higher loading ratios as well.

Unlike what we found at a 1:2 ratio and 1:4 ratio, there is no considerable difference between HFCs of FAs in site (B) of SRNS#3 samples and our reference adult samples. However, compared to the juvenile control sample, there is a difference in that 16-DSA at a 1:4 ratio shows a $\delta(2A'_{zz})$ of ∼6 MHz larger than the corresponding values of SRNS#3 and the healthy adult sample.

When inspecting the DLS and ELS data, there seem to be improvements in charge stability of the protein, evidenced by more negative zeta potential values when more FAs are bound, as it was reported before.[36] However, the particle sizes are still far larger than normal. The exact reason for this behavior is hard to pinpoint based on the recorded data sets and analysis thereof. One possible reason could be a partial unfolding of the protein. Note that DLS does not determine the actual particle size but the respective hydrodynamic diameter. With that in mind, it could be that the actual size of albumin is only slightly altered but water penetration into the protein is increased, and its hydration layer is far more extended, which would corroborate the finding of more water-exposed binding sites, found by EPR.

HSA:16-DSA 1:6. In the SRNS#3 sample series, both sites (A) and (B) are affected in terms of their HFC and dynamics at the high loading ratio of 1:6. They show higher HFCs at their (A) sites and lower values of HFC for their (B) sites, compared to both references (Table S2). Variations of

https://doi.org/10.1021/acs.jmedchem.3c00680
J. Med. Chem. 2023, 66, 12115−12129

SRNS#3's HFC in samples from all sampling dates and for all loading ratios are depicted in Figure S10.

We found similar trends of all changes in both, CW EPR and DLS data. SRNS#3.1(a+) presents albumin molecules with a significantly more negative zeta potential, observed at loading ratios 1:4 and higher. As discussed earlier, the sample might contain a high exogenous HSA fraction due to the infusion. Samples SRNS#3.2−3.5 show a reduced (more positive) zeta potential, featuring two major points: At low content of 16-DSA (loading ratio 1:2), the zeta potential for the SRNS#3-(a−) group is the most positive (see Figure 5). Note that both samples represent the state where the last albumin injection was 4 weeks ago so that exogenous HSA with a half-life time of less than 20 days does not contribute significantly to the tested albumin anymore and this reflects the endogenous HSA by this patient.

The moderate to strong instability of protein due to different charge distribution is also observed by light scattering techniques (more positive zeta potential by about 5−10 units and larger particle size) for all SRNS#3 samples and at all loading ratios. Note that sample SRNS#3.4(a+) had to be filtrated (see Materials section), which results in disturbing initially enlarged HSA particles, leading to smaller hydrodynamic radii values compared to all other SRNS#3 samples. HSA contains a significant portion of acidic surface-oriented residues, which makes the protein a negatively charged entity (−19 e at neutral pH). A possible deprotonation of these residues could explain such deviation from the charge stability of the protein. Increasing the concentration of 16-DSA increased the zeta potential to a more negative value close to the values of the "healthy" group and juvenile control samples. At the 1:6 loading ratio, all SRNS#3 samples (except for SRNS#3.1(a+)) present zeta potential values close to reference samples, whereas DLS data still present enlarged particle sizes (compared to monomeric HSA units). These results are in accordance with the known fact that the albumin tertiary structure is stabilized by binding FAs. Taken together, the severe PU in this patient may be due to the low filtration capacity of the GBM and the remarkably low interface charge of endogenous HSA. Injecting very large doses of exogenous and unmodified HSA counteracts this by adding HSA so that the PU can be moderated. Potentially, the endogenous HSA is still lost in large amounts, but the exogenously added HSA leads to a certain stability by not being lost (at least in large amounts) and hence leads to remission of the patient's state.

Clinical Interpretation. As far as we know this kind of physical−chemical investigation has not been performed before. Biomolecular investigations have described albumin modifications such as lipidated albumin, oxidized albumin, cationic albumin, and glycated albumin. Their functionality, electrokinetic potential, and ability to cross the filtration barrier, especially the negatively charged GBM as the main filtration barrier for albumin, have not been studied. Recent studies have shown that filtered amounts of albumin exhibit not only proximal tubulotoxicity but are also toxic for podocytes.[11] Biomolecular modifications of albumin such as lipidated albumin are even more toxic for podocytes.

Albumin that passes the glomerular filtration barrier can enter podocytes by micropinocytosis, caveolae-mediated endocytosis, or less by clathrin-mediated endocytosis: Albumin uptaken by podocytes may be degraded by lysosomes or bind to the neonatal Fc receptor FcRN, a transport receptor for albumin and IgG transcytosis.

Many glomerulopathies with nephrotic range proteinuria are caused by podocyte damage, inflammatory processes, or gene mutations of structures and functions essential for podocytes. Podocytes are the third barrier for the proper function of the filtration barrier and serve as a fine regulator. Their main function is, as described recently, to counteract the hydrostatic pressure of the glomerular capillary loops on the GBM and maintain their compression, which is essential for the filter function.[1]

The cause of SSNS and nongenetic FSGS is still not fully understood. Our experimental observations might point toward a new explanation for the clinical progression. We clearly show molecular alteration of albumin of patients with SSNS and nongenetic SRNS with an increase of the hydrodynamic radius, less negative zeta potential and, as shown by EPR, alterations in the strong and intermediate binding of spin-labeled FAs.

Overall, it is very likely that these alterations allow albumin to cross the filtration barrier to some extent and might be consequently uptaken by different endocytosis mechanisms. In combination with literature evidence highlighting the toxic effect of albumin on the cytoskeleton and complex structure/function of podocytes,[11] podocyte effacement and even detachment are consequences which are detectable by electron microscopy.

Therefore, the podocyte damage and effacement seen in SSNS and early FSGS may not be the cause for the NS, but the victim of altered HSA passing the GBM. This paradigm change is supported by the fact that patient SRNS#3 could be successfully treated by large amounts of exogenous molecular unaltered albumin superseding the diseased albumin, however, when interrupted may lead to relapse of the disease.

Since we could exclude a mutation of albumin gene, the reason for the albumin modification remains unclear. Posttranslational changes, modifications by cytokines, or exceeding binding capacities for toxic compounds must be considered. An understanding of the mechanism might lead to new therapeutic concepts.

CONCLUSIONS

The combined use of light scattering techniques (DLS and ELS) with EPR spectroscopy allows for unraveling variations in the interaction patterns between the FA 16-DSA and albumin in the blood serum of juvenile patients with different types of nephrotic syndrome. Moreover, we were able to analyze these interactions first in a simplified system (com-HSA) and transfer our approach to far more complex serum samples. We tried to clarify that there are differences between the HSA-FA binding behavior of protein modified by NS from healthy (control) HSA and their role in two studied groups of NS disease (SSNS and SRNS). Such alterations in proteins could be correlated to the measured changes in surface charge, internal protein environment, and structural changes of albumin itself. The latter, however, needs to be thoroughly investigated by other techniques like pulsed EPR methods (double electron-electron resonance and hyperfine spectroscopies), as we have shown before.[20,26]

By comparing the com-HSA system with the serum samples, categorized into the three patients groups with "no PU", "SSNS", and "SRNS", significant differences in the effective charge of the albumin were detected, especially at the low FA loading ratio of HSA:16-DSA 1:2. At this ratio, the main binding behavior of the FAs dominates the interaction pattern

https://doi.org/10.1021/acs.jmedchem.3c00680
J. Med. Chem. 2023, 66, 12115−12129

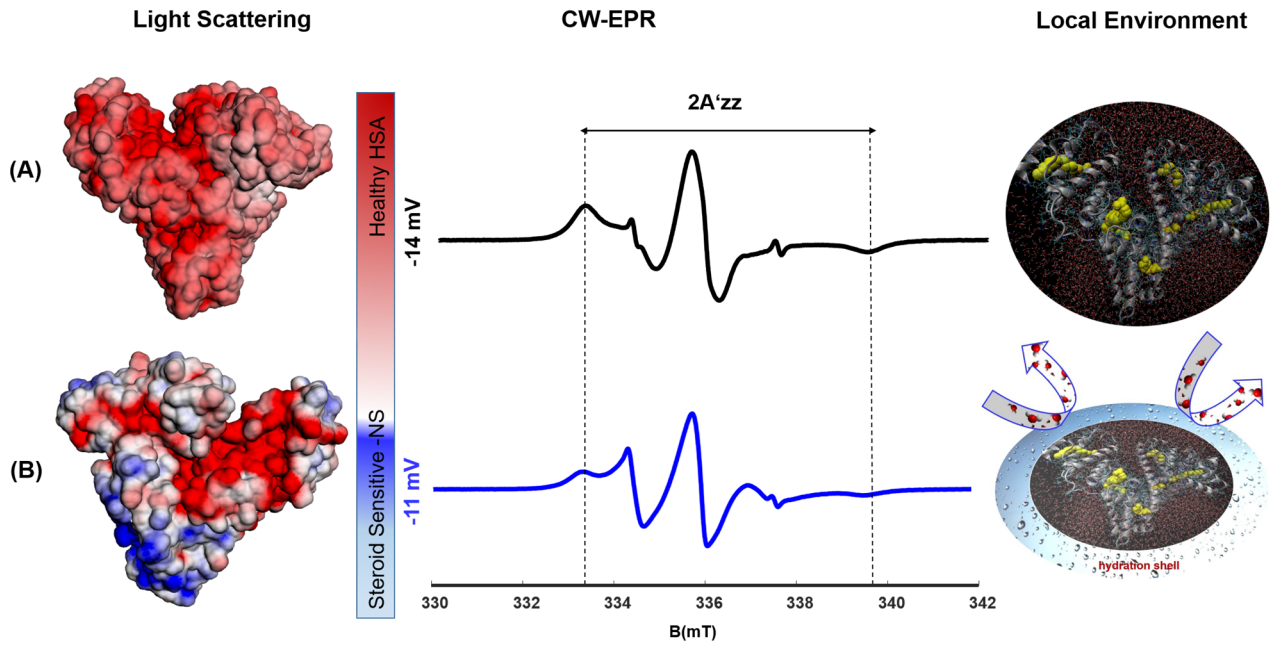

Figure 8. Graphical illustration of probed local environments via light scattering and CW-EPR. The two clearly discernible patient groups are (A) healthy and (B) steroid-sensitive-NS (SSNS). Left column: Calculated surface charges based on an APBS model (*Adaptive Poisson-Boltzmann Solver*) for the healthy structure.[51] The surface charges for two SSNS groups are adaptively scaled. Corresponding experimentally obtained zeta potentials (from DLS and ELS) at a 1:4 loading ratio of HSA:16-DSA are also given. As for the SSNS group, the average value of surface charges is given. Distribution of surface charges is color-coded in red (negative) and blue (positive). Middle column: Representative cw-EPR spectra at 1:4 loading ratio for each group show distinct differences in terms of both hyperfine coupling (indicative of FA binding behavior) and rotational correlation times (dynamics). Right column: Illustration of the local environment around HSA-bound FAs (shown in yellow) dissolved in water for healthy and NS-diseased groups.[52] The results from DLS and EPR on the SSNS group revealed a more hydrophobic environment around high-affinity binding sites of HSA. These data are depicted as pushing water molecules out of the surrounding hydration shell of the HSA molecule.

to albumin, presenting the following order for the absolute value (from less negative to more negative) of the measured zeta potential: SRNS < SSNS < no PU. The addition of steroids helps in the case of SSNS samples to partially regain the surface charge of the protein in the functional, healthy state. Increasing the loading ratio of 16-DSA induces similar effects, resulting in the vanishing of the differences in the zeta potential measurements (within the margin of error) for most of the serum samples. Exemptions were samples SRNS#1-mut+ and SRNS#3.1(a+), which possessed special medical conditions that altered the solution behavior of albumin even further.

In the case of the SSNS group, we found a direct correlation between the relatively positive effective charge of albumin and highly hydrophobic local surroundings as demonstrated via EPR spectroscopy. On the contrary, for the SRNS group, different mechanisms could be proposed to explain the differences. Permanent posttranslational changes in the binding behavior of albumin or strong binding of unknown biomarkers, as shown for sample SRNS#3, expose the protein interior to more water, resulting in possible further structural changes to compensate for the rendering/reordering of the solvent molecules around the protein.

Besides such structural changes, mutations in the *nphs1* gene coding for nephrin (SRNS#1-mut+) do not follow the described pattern of HSA. SRNS#2-mut− showed the smallest deviations in the SRNS group as compared to the controls. These findings are graphically summarized for the healthy and SSNS groups in Figure 8. Since we have three samples in the SRNS group, one of which is being monitored over the course of time and various additional states of exogenous HSA, we exclude this heterogeneous group from the simple graphical summary.

Interestingly, the addition of larger amounts of FAs (4 or 6 equivalents per HSA) seems—in all cases—to stabilize HSA functional, healthy structure also in serum samples. This effect has been characterized in vitro in purified HSA but is here shown in serum samples. One may speculate at this point that administration of substances binding to the FA binding sites of HSA might therefore ease the severity of diseases like NS that include severe PU and albumin loss, either due to posttranslational modifications of HSA or altered sieving characteristics through the GBM (Figure 1). Here, we propose a potential reason for the severe PU in some of these cases, which might change the view of the role of HSA in PU. However, expanding the group size and adding other laboratory techniques, such as mass spectrometry for the analysis of the posttranslational modifications in each patient's albumin, are needed to finally pinpoint how malfunctioning of albumin might trigger PU and whether diseased albumin is toxic to podocytes, leading to effacement of foot processes and enhances malfunction of the filtration barrier.[51,52]

EXPERIMENTAL SECTION

Sample Nomenclature. We have analyzed a total of 15 serum samples, 13 of which stem from the blood serum of children diagnosed with nephrotic syndrome, NS, provided by University Hospital Essen−Pediatric Clinic II. Informed consent was given by the parents to use left-over serum samples for the here reported exploratory investigations of unexplained clinical observations. For data protection, patients' identities were anonymized, and stored separately. Clinical data for all examined samples are shown in Table 1.

https://doi.org/10.1021/acs.jmedchem.3c00680
J. Med. Chem. 2023, 66, 12115−12129

Among these samples, one is of special interest (labeled SRNS#3 throughout the study). This patient developed nephrotic syndrome at the age of 1.5 years, which was resistant to steroids and all other drugs used to control this condition. Eventually, the patient developed renal failure, underwent dialysis, received a kidney transplant, and suffered an immediate relapse of nephrotic syndrome, which was again refractory to treatment except for high, almost daily HSA infusions. All serum samples provided were at various stages of treatment, as indicated on the label.

The sample received first (June 2017) is labeled as SRNS#3.1(a+) and refers to the state of the patient after transplantation with uncontrolled NS under high substitution of exogenous HSA. All other SRNS#3 samples are taken over the course of 2 years of sampling from 2017 until 2019.

For control, we used three different samples: One from a group of healthy adult samples provided by the Alfried Krupp Hospital in Essen that had been analyzed in detail in refs 25, 26. The second sample contains lyophilized powder of commercial, purified to 99%, FA-free human serum albumin (Sigma-Aldrich). These two samples, together with the sample of a juvenile patient without proteinuria served as "reference" samples. Throughout the text, we refer to samples containing commercial protein, as "commercial HSA" and "com-HSA", and the ones derived from patient's blood serum as HSA, unless otherwise mentioned.

16-DSA (>95%, Sigma-Aldrich) and aqueous glycerol solution (86−88 wt %, ACROS Organics) were used without further purification. Dulbecco's phosphate-buffered saline (DPBS) at pH 7.4 is used as a working buffer and is prepared thoroughly according to the original protocol.[53]

Albumin Concentration in Serum Samples. Blood samples were taken for diagnostic reasons by venipuncture. The time interval between sample collection and the following centrifugation was 15 min. After clotting, serum was separated by centrifugation (1000 × g) for 10 min at room temperature, removed, and then stored at −20 °C. The HSA concentration (g/dL) of all patients was measured by titration of a standard solution of the anionic dye bromcresol green to the albumin solution until a color change (blue-green complex) could be observed photometrically. Normal values are 3.5−5.0 g/dL; however, albumin levels in children are usually higher as they peak at age 20 and decline above age 60.[54]

Serum Sample Preparation for EPR and Light Scattering. It is well established that under physiological conditions, up to seven FAs can be taken up by HSA.[20,25] To provide paramagnetic centers necessary for EPR measurements, we employed spin-labeled 16-DSA as stearic acid-based FAs (Scheme S1 in the SI). For each patient serum sample, molar loading ratios of HSA:16-DSA were prepared from 1:1 to 1:7 in steps of 0.5 equivalents (12 samples in total). By applying molar ratios, we compensated for the fact that the received serum samples contain different stock concentrations of HSA. A 26 mM stock solution of 16-DSA in 0.1 M aqueous KOH was prepared from which the solutions with different loading ratios of HSA:16-DSA were made. The final HSA concentration was set to 200 μM by mixing the serum with DPBS buffer and glycerol solution such that the measured samples contained 20 wt % glycerol. Glycerol was used for internal comparability, to increase viscosity slightly to more resemble that of actual serum, as cryoprotectant during storage, and for potential later EPR measurements at cryogenic temperatures.[21] It can well be supposed that low-volume fractions of glycerol in fact integrate into water H-bonding structure and allow comparison with purely aqueous samples.[55] The final sample volume was 200 μL.

We used identical sets of samples for EPR, DLS, and ELS measurements so that the obtained results could be compared directly. However, one should note that for light scattering measurements, we had to dilute samples in a 1:1 (v/v) ratio with Milli-Q water (specific resistance of ρ = 18.2 MΩ cm) to reach a concentration of albumin with acceptable ionic strength. Therefore, the final HSA concentration for DLS and ELS was 100 μM and the ionic strength was between 50 and 60 mM. The addition of Milli-Q water reduces the glycerol content of the samples to 10 wt %, which still affects the viscosity (η), refractive index (n), and relative permittivity (ε_r) of the solution. These parameters are of importance for light scattering experiments and were adjusted to η = 1.17 mPas, n = 1.3420, and ε_r = 75.50 for all measurements accordingly.[56,57]

Commercial HSA Sample Preparation. As already established in previous studies with serum samples,[25] a comparison between HSA in serum and commercial HSA (com-HSA) in buffered solution is useful to resolve the induced interaction of albumin with added 16-DSA. It serves as both, a model compound for FA binding to HSA and indirectly characterizes albumin function by conducting EPR on the bound FAs. We probe the number of FAs bound to albumin as well as the binding mode (e.g., strong binding with rotational motion fully restricted on the EPR timescale), which both are suggested to have a main contribution in tubulointerstitial injury and podocytes injury.[28−30] For light scattering experiments, we prepared a sample series with com-HSA and the molar loading ratios of 1:1 to 1:7. The protein concentration was set to 120 μM and the ionic strength varied between 50 and 60 mM. Moreover, we tested one sample without FAs, labeled with a ratio of 1:0.

Dynamic Light Scattering. DLS measurements to characterize the hydrodynamic size of albumin in the serum samples as well as for the solutions with com-HSA were performed with a Litesizer 500 (Anton Paar GmbH, Graz, Austria). This device irradiates the samples, which are mounted on a temperature-controlled optical bench, with a semiconductor laser operating at λ = 658 nm. The intensity of the laser was automatically configured by the Litesizer 500 to record optimized count rate traces. We applied side (90°) and back (175°) scattering for our DLS measurements, which in general helps to analyze a broader range of samples with respect to shape anisotropies for the particle of interest.[33,35,58]

Quartz cells (Hellma Analytics, Müllheim, Germany) were used to measure all prepared samples. The samples were transported and stored frozen at −80 °C and were gently warmed up to room temperature for filling the sample cuvette. We refrained from filtering the serum samples into the quartz cell because we suspected blockage of the filter pores due to the larger-sized components in the serum. For sample SRNS#3.4(a+), we had to use filtration (pore size 0.45 μm) due to the presence of small aggregated species inside the prepared loading ratio solutions, which prevented the recording of reproducible autocorrelation functions. To prevent contamination such as dust inside the final solutions, we filtered all the additionally used solvents (like DPBS buffer) with Millex filter units (nylon membrane, pore size 0.20 μm). The measuring temperature was set to 25 °C, and an equilibration time of 1 min was allowed before starting the actual measurement. To analyze the recorded autocorrelation functions, we applied the ALV-5000/E/EPP software (v. 3.0.1.13, ALV-Laser-Vertriebsgesellschaft m.b.H. Langen, Germany). See the Supplementary Information (SI) for further details.

Due to the complex composition of the blood serum samples, we show all particle size distributions as mass-weighted traces. With this, the compounds with the largest volume/mass dominate the measurable contribution. In all tested serum samples, the peak corresponding to the albumin is the most pronounced one, allowing relative comparisons in the obtained hydrodynamic radii.

Electrophoretic Light Scattering. ELS was used to determine the zeta potential, also known as electrokinetic potential, of mobile particles during electrophoresis. The zeta potential, deduced from the electrophoretic mobility of the respective particles moving under an electric field, describes their potential at the slipping/shear plane.[35] This technique is often used in conjunction with DLS and the Litesizer 500 with its Kalliope software (v. 2.6) was used here for these measurements, too. Note that the Litesizer 500 utilizes continuously monitored Phase-Analysis Light Scattering (cmPALS), which is a more sophisticated version of ELS that allows evaluating the zeta potential for more sensitive samples like proteins.[59,60]

The prepared samples were measured with the so-called *Univette* (Anton Paar GmbH), which is a cuvette capable of characterizing samples with high conductivity and organic solvent content. To prevent Joule heating inside the measured samples, we reduced the applied voltage for the electric field to 8 V. A complete data set consists of three repetitive cmPALS measurements with a waiting

https://doi.org/10.1021/acs.jmedchem.3c00680
J. Med. Chem. 2023, 66, 12115−12129

period of 1 min between each run. The temperature was set to 25 °C. For data analysis, we used electrophoretic mobility as a directly accessible parameter and subsequently transferred it into the desired zeta potential. The exact process for calculating the electrokinetic potential was described previously[61,62] and can be found in the SI.

Continuous-Wave Electron Paramagnetic Resonance (CW EPR) Spectroscopy. All EPR spectra were recorded on a Magnettech MiniScope MS400 benchtop CW-EPR spectrometer (Magnettech, Berlin, Germany, now part of Bruker Biospin, Ettlingen, Germany) operating at X-band frequencies (9.43 GHz) at 298 K. A microwave power of 3.16 mW with a modulation frequency of 100 kHz, modulation amplitude of 0.1 mT and 4096 points were used throughout the measurements. The respective spectra were accumulated ten times, each for 60 s, yielding a final measurement time of 10 min per spectrum.

EPR spectra were simulated based on the spin Hamiltonian using the Easyspin software package (v. 5.2.25)[63] in MatLab (R2015b, v. 8.6). As described in previous studies on serum samples,[25,26] a three-component system was used for all simulations; strong affinity binding sites toward FAs that strongly immobilize bound FAs (hereafter called A-sites), intermediate affinity binding sites in which bound FAs show more rotational motion (B-sites) and nonbound, freely tumbling FAs. The principal values of the *g*-tensor were chosen according to the values reported for DOXYL-labeled stearic acids in interaction with bovine serum albumin.[64,65] To account for dynamics, this three-component system with anisotropic rotational mobility was considered for simulations, as detailed before in refs 66−68. To reduce complexity but to still have one meaningful value as a measure of rotational mobility, the reported rotational correlation times are calculated as a mean value based on an isotropic rotational model.[68] Simulation errors are calculated based on the root-mean-square (RMS)-deviations between experimental and simulated spectra for all spectral data points (4096 points).

Although the data for all loading ratios are available in the SI, herein, we focus on and discuss the results from three loading ratios of HSA:16-DSA; 1:2, 1:4, and 1:6. Each of these ratios can be considered to reflect characteristic behavior of the system consisting of protein and FA derivative; the 1:2 shows the main binding behavior, as at this ratio, of all FAs are bound and, at this concentration also, all binding sites are in principle occupied statistically (on average two per albumin). According to our former results,[25,26] the 1:4 ratio is the one at which prominent changes in FA binding become apparent and the 1:6 ratio is close to the case of the protein saturated with FAs.

■ ASSOCIATED CONTENT

Supporting Information

The Supporting Information is available free of charge at https://pubs.acs.org/doi/10.1021/acs.jmedchem.3c00680.

Analysis of Light Scattering Techniques; Dynamic Light Scattering (DLS) measurements; Electrophoretic Light Scattering (ELS) measurements; 16-Doxyl stearic acid (Scheme S1); Validate impact of DPBS concentration and glycerol on DLS (Figure S1); Summary of the DLS and ELS results (Table S1); Summary of EPR spectral simulation parameters (Tables S2, S3); Deconvolution of a multi-component spectrum (Figure S2); Experimental and simulation of EPR spectra (Figures S3, S4); Scatter dot plots of spectral contribution (Figures S5, S6); Boxplots of free (non-bound) fatty acids (Figure S7); Free components (non-bound fatty acids) per loading ratios (Figures S8, S9); Variation of hyperfine coupling (Figure S10); Scatter dot plots of 2A'zz (Figures S11, S12, S13) (PDF)

■ AUTHOR INFORMATION

Corresponding Authors

Peter Hoyer − *Universitätsklinikum Essen (AöR), Klinik für Kinderheilkunde II, Zentrum für Kinder- und Jugendmedizin, D-45147 Essen, Germany*; Email: peter.hoyer@uk-essen.de

Dariush Hinderberger − *Physical Chemistry, Complex Self-Organizing Systems, Martin Luther University Halle-Wittenberg, Institute of Chemistry, 06120 Halle (Saale), Germany*; orcid.org/0000-0002-6066-7099; Email: dariush.hinderberger@chemie.uni-halle.de

Authors

Haleh H. Haeri − *Physical Chemistry, Complex Self-Organizing Systems, Martin Luther University Halle-Wittenberg, Institute of Chemistry, 06120 Halle (Saale), Germany*

Jana Eisermann − *Department of Chemistry, Molecular Sciences Research Hub, Imperial College London, W12 0BZ London, U.K.*

Heike Schimm − *Physical Chemistry, Complex Self-Organizing Systems, Martin Luther University Halle-Wittenberg, Institute of Chemistry, 06120 Halle (Saale), Germany*

Anja Büscher − *Universitätsklinikum Essen (AöR), Klinik für Kinderheilkunde II, Zentrum für Kinder- und Jugendmedizin, D-45147 Essen, Germany*

Complete contact information is available at: https://pubs.acs.org/10.1021/acs.jmedchem.3c00680

Author Contributions

‖H.H.H. and J.E. contributed equally.

Author Contributions

A.B. and P.H. collected the blood serum samples and prepared the lab reports. Further sample preparations for actual DLS/ELS and EPR measurements was done by H.S. H.S. collected the CW-EPR data sets, which were simulated by H.H. J.E. performed DLS/ELS measurements and respective data analysis. D.H. and P.H. designed the research with contributions from H.H. and J.E. H.H. and J.E. wrote the manuscript with input from D.H. and P.H. All authors read and approved the final manuscript.

Notes

The authors declare no competing financial interest.

■ ACKNOWLEDGMENTS

We thank Annekatrin Schiebel for technical support.

■ ABBREVIATIONS

16-DSA, 16-doxyl stearic acid; CKD, chronic kidney diseases; DLS, Dynamic Light Scattering; ELS, Electrophoretic Light Scattering; EPR, Electron Paramagnetic Resonance; FA, fatty acid; FSGS, focal segmental glomerulosclerosis; GBM, glomerular basement membrane; HFC, apparent hyperfine coupling; HSA, human serum albumin; MCNS, minimal-change NS; NS, nephrotic syndrome; SRNS, steroid-resistant NS; SSNS, steroid-sensitive NS

■ REFERENCES

(1) Butt, L.; Unnersjö-Jess, D.; Höhne, M.; Edwards, A.; Binz-Lotter, J.; Reilly, D.; Hahnfeldt, R.; Ziegler, V.; Fremter, K.; Rinschen, M. M.; Helmstädter, M.; Ebert, L. K.; Castrop, H.; Hackl, M. J.; Walz, G.; Brinkkoetter, P. T.; Liebau, M. C.; Tory, K.; Hoyer, P. F.; Beck, B. B.;

Brismar, H.; Blom, H.; Schermer, B.; Benzing, T. A Molecular Mechanism Explaining Albuminuria in Kidney Disease. *Nat. Metab.* **2020**, *2*, 461−474.
(2) Eddy, A. A.; Symons, J. M. Nephrotic Syndrome in Childhood. *Lancet* **2003**, *362*, 629−639.
(3) Levin, M.; Smith, C.; Walters, M. D. S.; Gascoine, P.; Barratt, T. M. Steroid-Responsive Nephrotic Syndrome: A Generalised Disorder of Membrane Negative Charge. *Lancet* **1985**, *326*, 239−242.
(4) Hausmann, R.; Kuppe, C.; Egger, H.; Schweda, F.; Knecht, V.; Elger, M.; Menzel, S.; Somers, D.; Braun, G.; Fuss, A.; Uhlig, S.; Kriz, W.; Tanner, G.; Floege, J.; Moeller, M. J. Electrical Forces Determine Glomerular Permeability. *J. Am. Soc. Nephrol.* **2010**, *21*, 2053−2058.
(5) Carrie, B. J.; Salyer, W. R.; Myers, B. D. Minimal Change Nephropathy: An Electrochemical Disorder of the Glomerular Membrane. *Am. J. Med.* **1981**, *70*, 262−268.
(6) Königshausen, E.; Sellin, L. Recent Treatment Advances and New Trials in Adult Nephrotic Syndrome. *BioMed Res. Int.* **2017**, *2017*, No. 7689254.
(7) Russo, L. M.; Sandoval, R. M.; McKee, M.; Osicka, T. M.; Collins, A. B.; Brown, D.; Molitoris, B. A.; Comper, W. D. The Normal Kidney Filters Nephrotic Levels of Albumin Retrieved by Proximal Tubule Cells: Retrieval Is Disrupted in Nephrotic States. *Kidney Int.* **2007**, *71*, 504−513.
(8) Bentley, J.; Chande, H.; Kanigicherla, D.; Parker, K. Nephrotic Syndrome in Adults: Symptoms and Management. *Pharm. J.* **2021**, *306*, 43065.
(9) Hauenschild, T.; Reichenwallner, J.; Enkelmann, V.; Hinderberger, D. Characterizing Active Pharmaceutical Ingredient Binding to Human Serum Albumin by Spin-Labeling and EPR Spectroscopy. *Chem. − Eur. J.* **2016**, *22*, 12825−12838.
(10) McCloskey, O.; Maxwell, A. P. Diagnosis and Management of Nephrotic Syndrome. *Practitioner* **2017**, *261*, 11−15.
(11) Agrawal, S.; Smoyer, W. E. Role of Albumin and Its Modifications in Glomerular Injury. *Pflugers Arch. − Eur. J. Physiol.* **2017**, *469*, 975−982.
(12) Mortazavi, F.; Khiavi, Y. S. Steroid Response Pattern and Outcome of Pediatric Idiopathic Nephrotic Syndrome: A Single-Center Experience in Northwest Iran. *Ther. Clin. Risk Manage.* **2011**, *7*, 167−171.
(13) Deegens, J. K. J.; Dijkman, H. B. P. M.; Borm, G. F.; Steenbergen, E. J.; van den Berg, J. G.; Weening, J. J.; Wetzels, J. F. M. Podocyte Foot Process Effacement as a Diagnostic Tool in Focal Segmental Glomerulosclerosis. *Kidney Int.* **2008**, *74*, 1568−1576.
(14) Vivarelli, M.; Massella, L.; Ruggiero, B.; Emma, F. Minimal Change Disease. *Clin. J. Am. Soc. Nephrol.* **2017**, *12*, 332−345.
(15) Nicholson, J. P.; Wolmarans, M. R.; Park, G. R. The Role of Albumin in Critical Illness. *Br. J. Anaesth.* **2000**, *85*, 599−610.
(16) Quinlan, G. J.; Martin, G. S.; Evans, T. W. Albumin: Biochemical Properties and Therapeutic Potential. *Hepatology* **2005**, *41*, 1211−1219.
(17) Fasano, M.; Curry, S.; Terreno, E.; Galliano, M.; Fanali, G.; Narciso, P.; Notari, S.; Ascenzi, P. The Extraordinary Ligand Binding Properties of Human Serum Albumin. *IUBMB Life* **2005**, *57*, 787−796.
(18) Sebak, S.; Mirzaei, M.; Malhotra, M.; Kulamarva, A.; Prakash, S. Human Serum Albumin Nanoparticles as an Efficient Noscapine Drug Delivery System for Potential Use in Breast Cancer: Preparation and in Vitro Analysis. *Int. J. Nanomed.* **2010**, *5*, 525−532.
(19) Taboada, P.; Gutiérrez-Pichel, M.; Mosquera, V. Effects of the Molecular Structure of Two Amphiphilic Antidepressant Drugs on the Formation of Complexes with Human Serum Albumin. *Biomacromolecules* **2004**, *5*, 1116−1123.
(20) Reichenwallner, J.; Hinderberger, D. Using Bound Fatty Acids to Disclose the Functional Structure of Serum Albumin. *Biochim. Biophys. Acta, Gen. Subj.* **2013**, *1830*, 5382−5393.
(21) Reichenwallner, J.; Oehmichen, M.-T.; Schmelzer, C.; Hauenschild, T.; Kerth, A.; Hinderberger, D. Exploring the PH-Induced Functional Phase Space of Human Serum Albumin by EPR Spectroscopy. *Magnetochemistry* **2018**, *4*, 47.
(22) Swartz, H. M.; Khan, N.; Buckey, J.; Comi, R.; Gould, L.; Grinberg, O.; Hartford, A.; Hopf, H.; Hou, H.; Hug, E.; Iwasaki, A.; Lesniewski, P.; Salikhov, I.; Walczak, T. Clinical Applications of EPR: Overview and Perspectives. *NMR Biomed.* **2004**, *17*, 335−351.
(23) Klare, J. P. Biomedical Applications of Electron Paramagnetic Resonance (EPR) Spectroscopy. *Biomed. Spectrosc. and Imaging* **2012**, *1*, 101−124.
(24) Galazzo, L.; Meier, G.; Hadi Timachi, M.; Hutter, C. A. J.; Seeger, M. A.; Bordignon, E. Spin-Labeled Nanobodies as Protein Conformational Reporters for Electron Paramagnetic Resonance in Cellular Membranes. *Proc. Natl. Acad. Sci. U. S. A.* **2020**, *117*, 2441−2448.
(25) Haeri, H. H.; Schunk, B.; Tomaszewski, J.; Schimm, H.; Gelos, M. J.; Hinderberger, D. Fatty Acid Binding to Human Serum Albumin in Blood Serum Characterized by EPR Spectroscopy. *ChemistryOpen* **2019**, *8*, 650−656.
(26) Haeri, H. H.; Tomaszewski, J.; Phytides, B.; Schimm, H.; Möslein, G.; Niedergethmann, M.; Hinderberger, D.; Gelos, M. Identification of Patients with Pancreatic Cancer by Electron Paramagnetic Resonance Spectroscopy of Fatty Acid Binding to Human Serum Albumin. *ACS Pharmacol. Transl. Sci.* **2020**, *3*, 1188−1198.
(27) Hinderberger, D.; Jeschke, G. Site-Specific Characterization of Structure and Dynamics of Complex Materials by EPR Spin Probes. In *Modern Magnetic Resonance*; Webb, G. A., Ed.; Springer Netherlands: Dordrecht, 2006; pp 1529−1537.
(28) Agrawal, S.; Guess, A. J.; Chanley, M. A.; Smoyer, W. E. Albumin-Induced Podocyte Injury and Protection Are Associated with Regulation of COX-2. *Kidney Int.* **2014**, *86*, 1150−1160.
(29) Allison, S. J. Free Fatty Acid-Induced Macropinocytosis in Podocytes. *Nat. Rev. Nephrol.* **2015**, *11*, 386−386.
(30) Chung, J.-J.; Huber, T. B.; Gödel, M.; Jarad, G.; Hartleben, B.; Kwoh, C.; Keil, A.; Karpitskiy, A.; Hu, J.; Huh, C. J.; Cella, M.; Gross, R. W.; Miner, J. H.; Shaw, A. S. Albumin-Associated Free Fatty Acids Induce Macropinocytosis in Podocytes. *J. Clin. Invest.* **2015**, *125*, 2307−2316.
(31) Ghiggeri, G. M.; Ginevri, F.; Candiano, G.; Oleggini, R.; Perfumo, F.; Queirolo, C.; Gusmano, R. Characterization of Cationic Albumin in Minimal Change Nephropathy. *Kidney Int.* **1987**, *32*, 547−553.
(32) Debiec, H.; Lefeu, F.; Kemper, M. J.; Niaudet, P.; Deschênes, G.; Remuzzi, G.; Ulinski, T.; Ronco, P. Early-Childhood Membranous Nephropathy Due to Cationic Bovine Serum Albumin. *N. Engl. J. Med.* **2011**, *364*, 2101−2110.
(33) Pecora, R. Dynamic Light Scattering Measurement of Nanometer Particles in Liquids. *J. Nanopart. Res.* **2000**, *2*, 123−131.
(34) Stetefeld, J.; McKenna, S. A.; Patel, T. R. Dynamic Light Scattering: A Practical Guide and Applications in Biomedical Sciences. *Biophys. Rev.* **2016**, *8*, 409−427.
(35) Bhattacharjee, S. DLS and Zeta Potential - What They Are and What They Are Not? *J. Controlled Release* **2016**, *235*, 337−351.
(36) Jachimska, B.; Wasilewska, M.; Adamczyk, Z. Characterization of Globular Protein Solutions by Dynamic Light Scattering, Electrophoretic Mobility, and Viscosity Measurements. *Langmuir* **2008**, *24*, 6867−6872.
(37) Delgado, A. V.; González-Caballero, F.; Hunter, R. J.; Koopal, L. K.; Lyklema, J. Measurement and Interpretation of Electrokinetic Phenomena: (IUPAC Technical Report). *Pure Appl. Chem.* **2005**, *77*, 1753−1805.
(38) Leggio, C.; Galantini, L.; Pavel, N. V. About the Albumin Structure in Solution: Cigar Expanded Form versus Heart Normal Shape. *Phys. Chem. Chem. Phys.* **2008**, *10*, 6741−6750.
(39) Spector, A. A. Fatty Acid Binding to Plasma Albumin. *J. Lipid Res.* **1975**, *16*, 165−179.
(40) Ma, G. J.; Ferhan, A. R.; Jackman, J. A.; Cho, N.-J. Conformational Flexibility of Fatty Acid-Free Bovine Serum Albumin Proteins Enables Superior Antifouling Coatings. *Commun. Mater.* **2020**, *1*, 45.

https://doi.org/10.1021/acs.jmedchem.3c00680
J. Med. Chem. 2023, 66, 12115−12129

(41) Philippe, A.; Nevo, F.; Esquivel, E. L.; Reklaityte, D.; Gribouval, O.; Tête, M. J. P.; Loirat, C.; Dantal, J.; Fischbach, M.; Pouteil-Noble, C.; Decramer, S.; Hoehne, M.; Benzing, T.; Charbit, M.; Niaudet, P.; Antignac, C. Nephrin Mutations Can Cause Childhood-Onset Steroid-Resistant Nephrotic Syndrome. *J. Am. Soc. Nephrol.* **2008**, *19*, 1871−1878.
(42) Saracino, G. A. A.; Tedeschi, A.; D'Errico, G.; Improta, R.; Franco, L.; Ruzzi, M.; Corvaia, C.; Barone, V. Solvent Polarity and PH Effects on the Magnetic Properties of Ionizable Nitroxide Radicals: A Combined Computational and Experimental Study of 2,2,5,5-Tetramethyl-3-Carboxypyrrolidine and 2,2,6,6-Tetramethyl-4-Carboxypiperidine Nitroxides. *J. Phys. Chem. A* **2002**, *106*, 10700−10706.
(43) Pavone, M.; Cimino, P.; Crescenzi, O.; Sillanpä, A.; Barone, V. Interplay of Intrinsic, Environmental, and Dynamic Effects in Tuning the EPR Parameters of Nitroxides: Further Insights from an Integrated Computational Approach. *J. Phys. Chem. B* **2007**, *111*, 8928−8939.
(44) Simard, J. R.; Zunszain, P. A.; Ha, C. E.; Yang, J. S.; Bhagavan, N. V.; Petitpas, I.; Curry, S.; Hamilton, J. A. Locating High-Affinity Fatty Acid-Binding Sites on Albumin by x-Ray Crystallography and NMR Spectroscopy. *Proc. Natl. Acad. Sci. U. S. A.* **2005**, *102*, 17958−17963.
(45) Simard, J. R.; Zunszain, P. A.; Hamilton, J. A.; Curry, S. Location of High and Low Affinity Fatty Acid Binding Sites on Human Serum Albumin Revealed by NMR Drug-Competition Analysis. *J. Mol. Biol.* **2006**, *361*, 336−351.
(46) Lowenthal, M. S.; Mehta, A. I.; Frogale, K.; Bandle, R. W.; Araujo, R. P.; Hood, B. L.; Veenstra, T. D.; Conrads, T. P.; Goldsmith, P.; Fishman, D.; Petricoin, E. F.; Liotta, L. A. Analysis of Albumin-Associated Peptides and Proteins from Ovarian Cancer Patients. *Clin. Chem.* **2005**, *51*, 1933−1945.
(47) Gurachevsky, A.; Muravskaya, E.; Gurachevskaya, T.; Smirnova, L.; Muravsky, V. Cancer-Associated Alteration in Fatty Acid Binding to Albumin Studied by Spin-Label Electron Spin Resonance. *Cancer Invest.* **2007**, *25*, 378−383.
(48) Kazmierczak, S. C.; Gurachevsky, A.; Matthes, G.; Muravsky, V. Electron Spin Resonance Spectroscopy of Serum Albumin: A Novel New Test for Cancer Diagnosis and Monitoring. *Clin. Chem.* **2006**, *52*, 2129−2134.
(49) Gelos, M.; Hinderberger, D.; Welsing, E.; Belting, J.; Schnurr, K.; Mann, B. Analysis of Albumin Fatty Acid Binding Capacity in Patients with Benign and Malignant Colorectal Diseases Using Electron Spin Resonance (ESR) Spectroscopy. *Int. J. Colorectal Dis.* **2010**, *25*, 119−127.
(50) Matricon, P.; Suresh, R. R.; Gao, Z. G.; Panel, N.; Jacobson, K. A.; Carlsson, J. Ligand Design by Targeting a Binding Site Water. *Chem. Sci.* **2021**, *12*, 960−968.
(51) Jurrus, E.; Engel, D.; Star, K.; Monson, K.; Brandi, J.; Felberg, L. E.; Brookes, D. H.; Wilson, L.; Chen, J.; Liles, K.; Chun, M.; Li, P.; Gohara, D. W.; Dolinsky, T.; Konecny, R.; Koes, D. R.; Nielsen, J. E.; Head-Gordon, T.; Geng, W.; Krasny, R.; Wei, G. W.; Holst, M. J.; McCammon, J. A.; Baker, N. A. Improvements to the APBS Biomolecular Solvation Software Suite. *Protein Sci.* **2018**, *27*, 112−128.
(52) Humphrey, W.; Dalke, A.; Schulten, K. VMD: Visual Molecular Dynamics. *J. Mol. Graphics* **1996**, *14* (October 1995), 33−38.
(53) Dulbecco, R.; Vogt, M. Plaque Formation and Isolation of Pure Lines with Polymyelits Viruses. *J. Exp. Med.* **1954**, *99*, 167−182.
(54) Weaving, G.; Batstone, G. F.; Jones, R. G. Age and Sex Variation in Serum Albumin Concentration: An Observational Study. *Ann. Clin. Biochem.* **2016**, *53*, 106−111.
(55) Hunold, J.; Eisermann, J.; Brehm, M.; Hinderberger, D. Characterization of Aqueous Lower-Polarity Solvation Shells Around Amphiphilic 2,2,6,6-Tetramethylpiperidine-1-Oxyl Radicals in Water. *J. Phys. Chem. B* **2020**, *124*, 8601−8609.
(56) Kuila, D. K.; Lahiri, S. C. Comparison of the Macroscopic Molecular Properties in Understanding the Structural Aspects of Mixed Aquo-Organic Binary Mixtures. *Z. Phys. Chem.* **2004**, *218*, 803−828.
(57) Wohlfarth, Ch.; Wohlfahrt, B. *Pure Organometallic and Organononmetallic Liquids, Binary Liquid Mixtures*; Lechner, M. D., Ed.; Springer-Verlag: Berlin, Heidelberg, 2001.
(58) Hassan, P. A.; Rana, S.; Verma, G. Making Sense of Brownian Motion: Colloid Characterization by Dynamic Light Scattering. *Langmuir* **2015**, *31*, 3−12.
(59) Noack, Harald; Moitzi, C. Modulator Monitoring During Measuring Electromobility, US 2014/0144780 A1, United States, 2014.
(60) Tscharnuter, W. W.; McNeil-Watson, F.; Fairhurst, D. A New Instrument for the Measurement of Very Small Electrophoretic Mobilities Using Phase Analysis Light Scattering. *ACS Symp. Ser.* **1998**, *693*, 327−340.
(61) Eisermann, J.; Kerth, A.; Hinderberger, D. Dynamic Self-Assembly of Ions with Variable Size and Charge in Solution. *RSC Adv.* **2019**, *9*, 18627−18640.
(62) Reichenwallner, J.; Thomas, A.; Steinbach, T.; Eisermann, J.; Schmelzer, C. E. H.; Wurm, F.; Hinderberger, D. Ligand-Binding Cooperativity Effects in Polymer-Protein Conjugation. *Biomacromolecules* **2019**, *20*, 1118−1131.
(63) Stoll, S.; Schweiger, A. EasySpin, a Comprehensive Software Package for Spectral Simulation and Analysis in EPR. *J. Magn. Reson.* **2006**, *178*, 42−55.
(64) Shenkar, M. G.; Rananavare, B.; Freed, J. H. ESR Studies of Stearic Acid Binding to Bovine Serum Albumin. *Biochim. Biophys. Acta, Gen. Subj.* **1990**, *1036*, 228−236.
(65) Earle, K. A.; Budil, D. E.; Freed, J. H. 250-GHz EPR of Nitroxides in the Slow-Motional Regime: Models of Rotational Diffusion. *J. Phys. Chem.* **1993**, *97*, 13289−13297.
(66) Freed, J. H. Anisotropic Rotational Diffusion and Electron Spin Resonance Linewidths. *J. Chem. Phys.* **1964**, *41*, 2077−2083.
(67) Freed, J. H. Theory of Slow Tumbling ESR Spectra for Nitroxides. In *Spin-Labeling: Theory and Application*; Berliner, L. J., Ed.; Academic Press Inc.: New York, 1976; pp 53−130.
(68) Oppenheim, S. F.; Buettner, G. R.; Rodgers, V. G. J. Relationship of Rotational Correlation Time from EPR Spectroscopy and Protein-Membrane Interaction. *J. Membr. Sci.* **1996**, *118*, 133−139.

https://doi.org/10.1021/acs.jmedchem.3c00680
J. Med. Chem. 2023, 66, 12115−12129